SUPPORTED PUNCH SHEAR BEHAVIOUR OF POLYCARBONATE: TEST, ANALYSIS AND NUMERICAL SIMULATION

Yunfa Zhang, Qi Yang, Richard Desnoyers, Andrew Johnston

Aerospace Research Centre, National Research Council Canada
1200 Montreal Road, Ottawa, ON, Canada K1A 0R6

ABSTRACT

This paper presents the results of an investigation into the punch shear behaviour of polycarbonate. First, supported punch shear tests were carried out using injection moulded disk specimens. Ductile material behaviour was observed during the punch shear process which consisted of an elastic stage, a prolonged deformation stage, and an abrupt shear-out stage at a large displacement. The complex damage mode was investigated with the aid of scanning electron microscopy. Notably, it was found that a circumferential tensile crack existed in the punched-out specimen, indicating that tensile deformation played an important role in the punch shear process. An axisymmetric simple shear model was established assuming a uniform deformation mode. The kinematic analysis indicated that very large shear and normal strains occurred at high loads, validating the test observation that both tensile and shear damage can occur during punch shear. In addition, a finite element analysis accounting for the large deformation effect was performed. The predicted results of the average shear stress versus normalized displacement curves were in good agreement with the test results and the numerical results revealed that the punch tool clearance had a considerable influence on the punch shear response. Finally, the identification of the potential damage location and the evolution of the local plastic deformation were demonstrated.

1. INTRODUCTION

Polycarbonate is a transparent thermoplastic [1] commonly used in lightweight armour and other applications ranging from safety goggles to aircraft windshields. Polycarbonate possesses an unusually high ballistic resistance to penetration and perforation due to its high ductility and high strength over a wide range of strain rates and temperatures. Shear properties have been identified as playing a significant role in the energy absorption behaviour during ballistic impact on polymers and composite laminates. Several well established test approaches are available to characterize the shear behaviour of polymers and fibre composites, which include: torsion of thin-walled tubes, Iosipescu shear, V-notched rail shear, and punch shear [2-4]. In particular, the punch shear test approach is widely employed to determine the through thickness shear properties of polymers and composites, especially for materials in sheet form [3-4].

Liu and Piggott [4-6] evaluated the shear strengths of several thermoplastic polymers (including polycarbonate) as well as epoxy materials employing both punch shear and Iosipescu shear

SAMPE Conference Proceedings. Charlotte, NC, May 20-23, 2019. Society for the Advancement of Material and Process Engineering – North America.

approaches. It was concluded that the punch shear test may provide more reliable results. They also found that a circumferential tensile type crack existed in the plugged-out part of the polycarbonate, polyvinyl chloride, polymethyl methacrylate and polyamide specimens tested in punch shear [6]. Mitsomwang and Nagasawa [7] studied the cutting characteristics of a thin polycarbonate sheet subjected to a straight punch/die shearing. The punch tool clearance and feed speed of the shearing process were varied and investigated. Dynamic punch tests of polycarbonate have also been investigated by a number of researchers [8-9]. Husain et al. [8] studied the response of polycarbonate plate subjected to normal impact by blunt and truncated cone projectiles experimentally and numerically. They found that more energy was absorbed in the shear plugging process with the blunt projectile as compared to the truncated cone projectile. Bilyk [9] presented a detailed computational analysis of the dynamic punch shear test using the Arbitrary-Lagrangian-Eulerian code ALEGRA. The validity of a conventional viscoplastic constitutive relation and the failure criterion for polycarbonate was determined based on their ability to predict the observed mechanical response. Finally, it is noticed that a number of researchers have developed ballistic penetration models for fibre composites based on the results of the punch shear test [10-12].

This investigation consists of test, analysis and numerical simulation of the punch shear behaviour of polycarbonate. In the experimental study, supported punch shear tests were carried out on injection moulded disk specimens. Ductile behaviour of the materials was demonstrated by the load versus displacement curves and damage mode was examined with the aid of scanning electron microscopy (SEM). To understand the complex damage behaviour observed in the test, a simplified axisymmetric model was established in which a uniform deformation in simple shear mode is assumed. The kinematic analysis reveals that significantly large shear and normal strains exist at high load levels. Finally, a nonlinear finite element analysis accounting for the large deformation effect was performed. The influence of the punch tool clearance on the punch shear response was studied and the predicted results of average shear stress versus displacement curves were compared with available test results. Moreover, the potential damage location and the evolution of the plastic deformation were also illustrated.

2. PUNCH SHEAR TEST OF POLYCARBONATE

2.1 Experimental

Polycarbonate Lexan 143R, an injection grade polycarbonate, was employed to fabricate the punch shear test specimens. Circular disk specimens of 63 mm in diameter and 3 mm thick were produced using injection moulding.

Figure 1(a) illustrates the schematic drawing of the supported punch shear test setup employed in the present investigation [3-4]. The central portion of the disk specimen is clamped in the punch assembly (highlighted in blue color in Figure 1a) using a threaded fastener through a central hole in the specimen. The outer portion of the specimen is then clamped between two rigid steel blocks. By pushing the punch assembly using a material testing machine, the inner portion of the specimen moves downward relative to the fixed outer portion, producing a shear deformation through the thickness of the specimen. In this study, all the punch shear tests were carried out using a load-frame at a crosshead speed of 1.25 mm/minute [3]. Figure 1(b) demonstrates a deformed specimen in which the central portion is sheared out from the specimen.

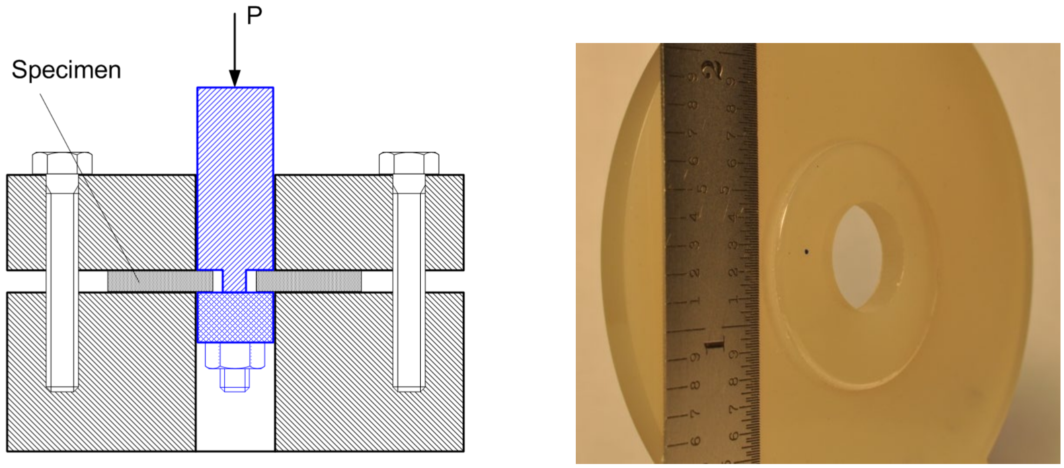

(a) (b)

Figure 1. (a) Punch shear test setup; (b) Plugging out of the central part of the specimen.

2.2 Test Results

Figure 2 represents the average shear stress versus the normalized displacement curves of three specimens obtained from the supported punch shear. As shown in the figure, the punch shear process consists of an elastic stage, a prolonged deformation stage, and an abrupt shear-out stage at large displacement. There are an obvious first peak load (P_1) and a maximum peak load (P_{max}) which correspond to the average yield strength and average shear strength of the material, respectively. The average yield strength obtained is 38.8 MPa and the shear strength is 77.0 MPa, indicating a significant hardening effect beyond yielding.

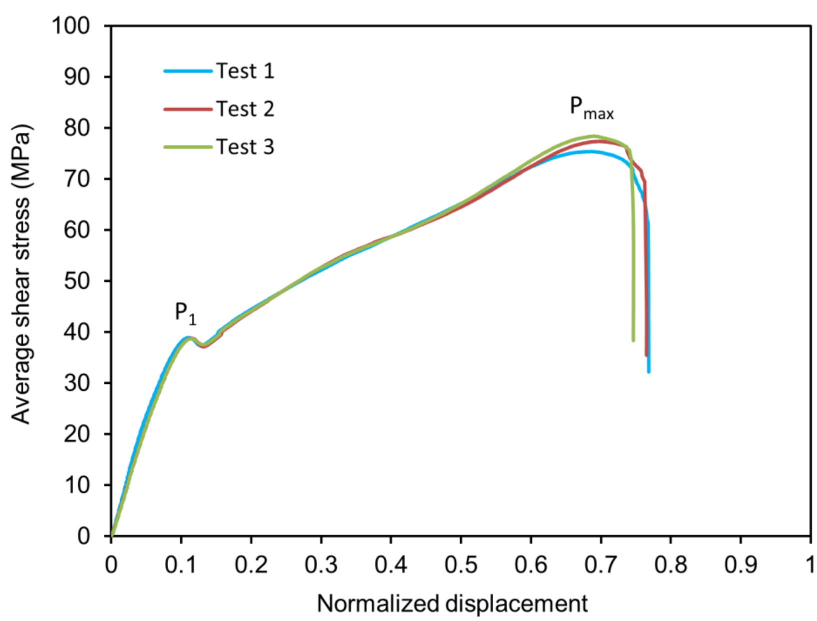

Figure 2. Average shear stress versus normalized displacement curves.

Further loading beyond the maximum load would result in a ring being plugged out from the disk specimen. This ring consists of two damage zones ("I" and "II" in Figure 3a) on the shear surface, separated by a circumferential crack. The two damage zones are identified by the very different roughness, as shown in the SEM image in Figure 3(b).

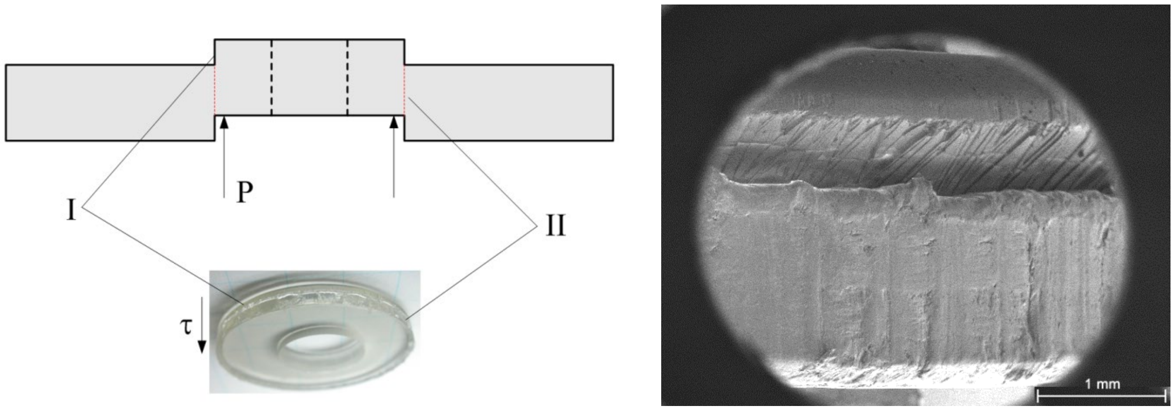

(a) (b)

Figure 3. (a) Schematic of punch shear; (b) SEM of sheared-out ring showing different damage zones.

Figure 4(a) represents an SEM image with a higher magnification for the cracked surface in zone "I" of the polycarbonate specimen. Obvious ridges and valleys on the surface show the representative tensile crack surface. On the other hand, as shown in Figure 4(b), there are no obvious oriented damage bands in the damage zone "II" and the surface is fairly smooth.

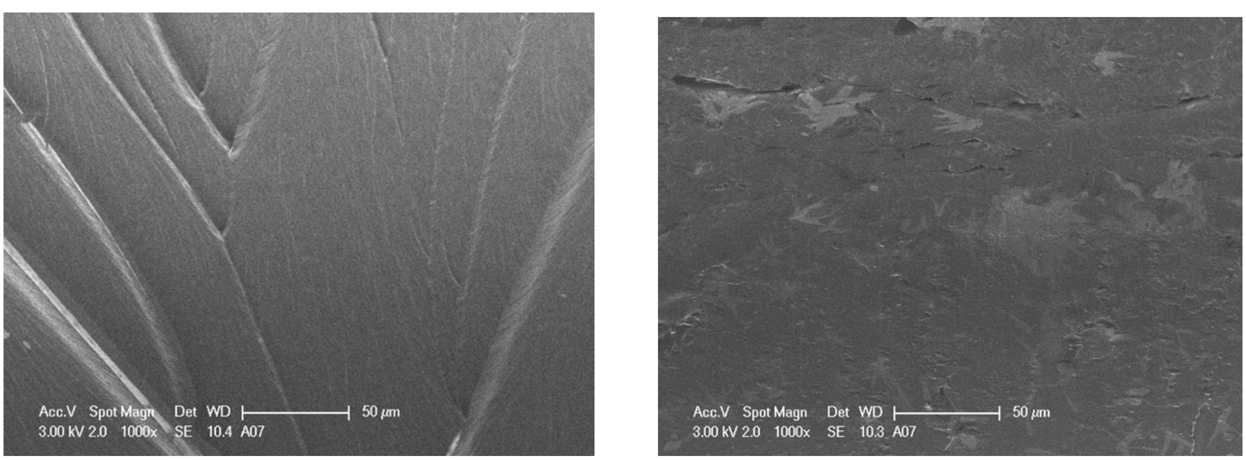

(a) (b)

Figure 4. (a) Surface of damage zone "I"; (b) Surface of damage zone "II".

3. SIMPLIFIED ANALYSIS OF AXISYMMETRIC SIMPLE SHEAR

3.1 Model and Analysis

The punch shear process of the disk specimen depicted in Figure 1 can be assumed to be under an idealized axisymmetric condition. In addition, it was observed that the deformation was localized in a very narrow zone which is induced by a usual very small clearance (δ) between the punch assembly and the fixed steel blocks [3-4, 7]. Therefore a simplified axisymmetric model shown in Figure 5 is established to allow a kinematic analysis using the large deformation theory. It should be noted that the uniform deformation mode is similar to the well-known simple shear deformation in 2-dimensions [13-15]. Hence herein it is referred to as axisymmetric simple shear.

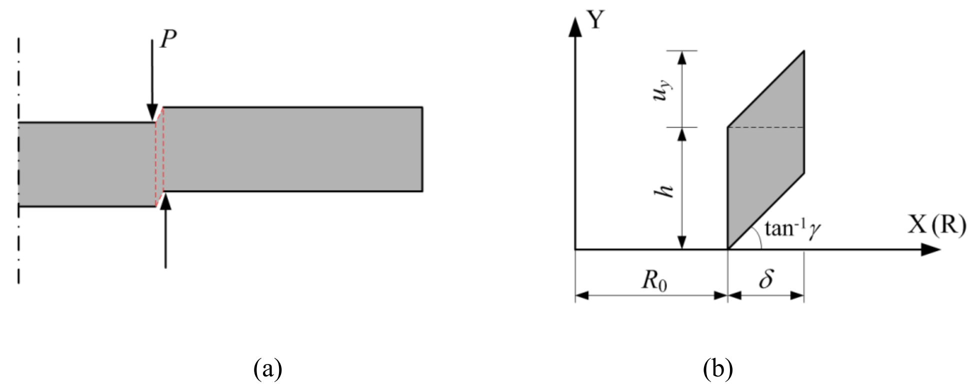

Figure 5. (a) Simplified punch shear scheme (not in actual scale); (b) Axisymmetric simple shear deformation of an element of thickness h.

Let **X** and **x** denote the position vectors of an arbitrary material point in the reference and deformed configurations, respectively. As illustrated in Figure 5(b), the deformation of the simplified shear process (with displacement **u**) can be described by

$$\mathbf{x} = \mathbf{X} + \mathbf{u} = X\boldsymbol{l} + [Y + \gamma(X - R_0)]\boldsymbol{m} + Z\boldsymbol{n} \qquad [1]$$

where X, Y, Z are the coordinates in the reference configuration and $\boldsymbol{l}$, $\boldsymbol{m}$, $\boldsymbol{n}$ are the unit vectors of the global coordinate system. Designating δ as the width of the material element in shear and u_y as the displacement in the axial direction (Y), respectively, we have

$$\gamma = u_y/\delta \qquad [2]$$

The deformation gradient tensor **F** can therefore be determined as

$$\mathbf{F} = \boldsymbol{l}\otimes\boldsymbol{l} + \boldsymbol{m}\otimes\boldsymbol{m} + \boldsymbol{n}\otimes\boldsymbol{n} + \gamma\boldsymbol{m}\otimes\boldsymbol{l} \qquad [3]$$

The right Cauchy-Green deformation tensor [15] is defined by $\mathbf{C} = \mathbf{F}^T\mathbf{F}$, where T denotes the transpose. Using Equation [3], we have

$$\mathbf{C} = (1 + \gamma^2)\boldsymbol{l}\otimes\boldsymbol{l} + \boldsymbol{m}\otimes\boldsymbol{m} + \boldsymbol{n}\otimes\boldsymbol{n} + \gamma(\boldsymbol{l}\otimes\boldsymbol{m} + \boldsymbol{m}\otimes\boldsymbol{l}) \qquad [4]$$

Therefore the Lagrange strain tensor [15] is

$$\mathbf{E} = \frac{1}{2}(\mathbf{C} - \mathbf{I}) = \frac{1}{2}\gamma^2 \boldsymbol{l}\otimes\boldsymbol{l} + \frac{1}{2}\gamma(\boldsymbol{l}\otimes\boldsymbol{m} + \boldsymbol{m}\otimes\boldsymbol{l}) \qquad [5]$$

where **I** is the identity tensor. Recalling Equation [2], the non-zero strain components are

$$\begin{cases} E_{xx} = \frac{1}{2}\gamma^2 = \frac{1}{2}\left(u_y/\delta\right)^2 \\ E_{xy} = \frac{1}{2}\gamma = \frac{1}{2}(u_y/\delta) \\ E_{yx} = E_{xy} \end{cases} \qquad [6]$$

It is seen that a normal strain component (E_{xx}) exists in the deformation, although the global loading is axisymmetric simple shear (Figure 5b).

According to the polar decomposition theorem [15], the deformation gradient tensor **F** can be decomposed into a product of two tensors as

$$\mathbf{F} = \mathbf{RU} \qquad [7]$$

where **R** is a proper orthogonal tensor ($\mathbf{R}^T = \mathbf{R}^{-1}$) and **U** is the right stretch tensor. The eigenvalues of **U** are the principal stretches of the deformation since **U** is positive definite and symmetric. For the present deformation in axisymmetric simple shear, we have

$$\mathbf{U} = \lambda_1 \boldsymbol{p_1}\otimes\boldsymbol{p_1} + \lambda_2 \boldsymbol{p_2}\otimes\boldsymbol{p_2} + \lambda_3 \boldsymbol{p_3}\otimes\boldsymbol{p_3} \qquad [8]$$

where the principal stretches ($\lambda_1 \geq \lambda_2 \geq \lambda_3$) are expressed as

$$\begin{cases} \lambda_1 = \left(1 + \frac{1}{4}\gamma^2\right)^{1/2} + \frac{1}{2}\gamma \\ \lambda_2 = 1 \\ \lambda_3 = \lambda_1^{-1} \end{cases} \qquad [9]$$

Moreover, the orientations of the principal stretches are specified by the proper vectors $\boldsymbol{p}_1$, $\boldsymbol{p}_2$, and $\boldsymbol{p}_3$ as

$$\begin{cases} \boldsymbol{p}_1 = cos\theta\boldsymbol{l} + sin\theta\boldsymbol{m} \\ \boldsymbol{p}_2 = \boldsymbol{n} \\ \boldsymbol{p}_3 = -sin\theta\boldsymbol{l} + cos\theta\boldsymbol{m} \end{cases} \qquad [10]$$

with

$$\theta = \frac{1}{2}tan^{-1}(2/\gamma) \qquad (0 < \theta < \pi/4) \qquad [11]$$

3.2 Illustrative Results

Figure 6 plots the strain components (Equation 6) versus the applied displacement for $\delta/h = 0.05$. It can be seen that both normal and shear strains appear in the shear process. As expressed in Equation [6] and shown in Figure 6, shear strain E_{xy} varies with the displacement proportionally while the normal strain E_{xx} varying quadratically. As indicated by the inset in Figure 6, when the displacement is small, the dominant strain component is the shear strain E_{xy}, as expected. However, at large displacement, both E_{xx} and E_{xy} can be significantly large. Thus, a tensile type failure is possible at large deformation.

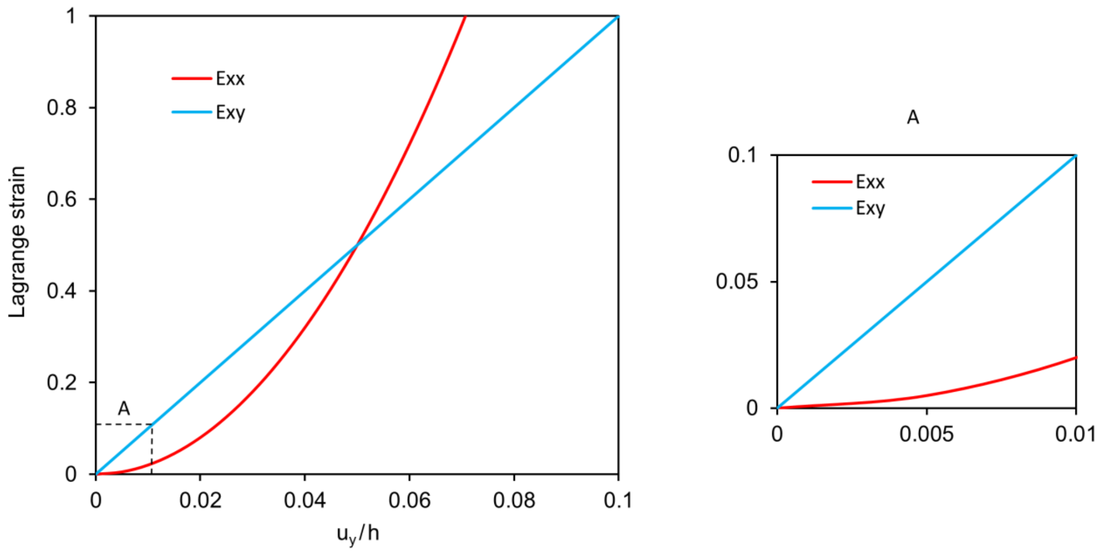

Figure 6. Comparison of normal and shear strain components in axisymmetric simple shear.

Figure 7 depicts the orientation angle (Equation 11) of the first principal stretch versus the displacement for different δ. It shows that at large deformations the inclination angle of the principal stretch to the radial direction (X) could be very small. As shown in the subsequent discussion, this angle describes the orientation of tensile cracks in the punch shear.

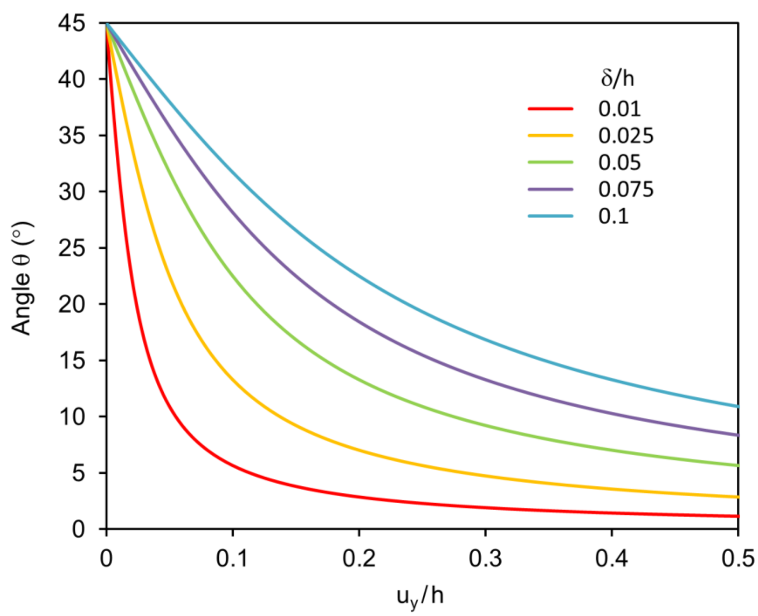

Figure 7. Orientation angle of the first principal stretch.

Figure 8 represents an SEM image of the central portion of a specimen completely plugged out from the original disk (See Section 2 for the details of the test setup). The orientation angle of the principal stretch is also shown in the inset in the figure. A circumferential opening crack is observed at approximately one third of the specimen thickness, along with a quite smooth surface produced by shear. Similar crack modes in punch shear for polycarbonate and ultra-high molecular weight polyethylene polymers were reported by Liu and Piggott [6], and Kurtz et al. [16], respectively. The present simplified analysis provides an explanation of this unique damage mode in punch shear test.

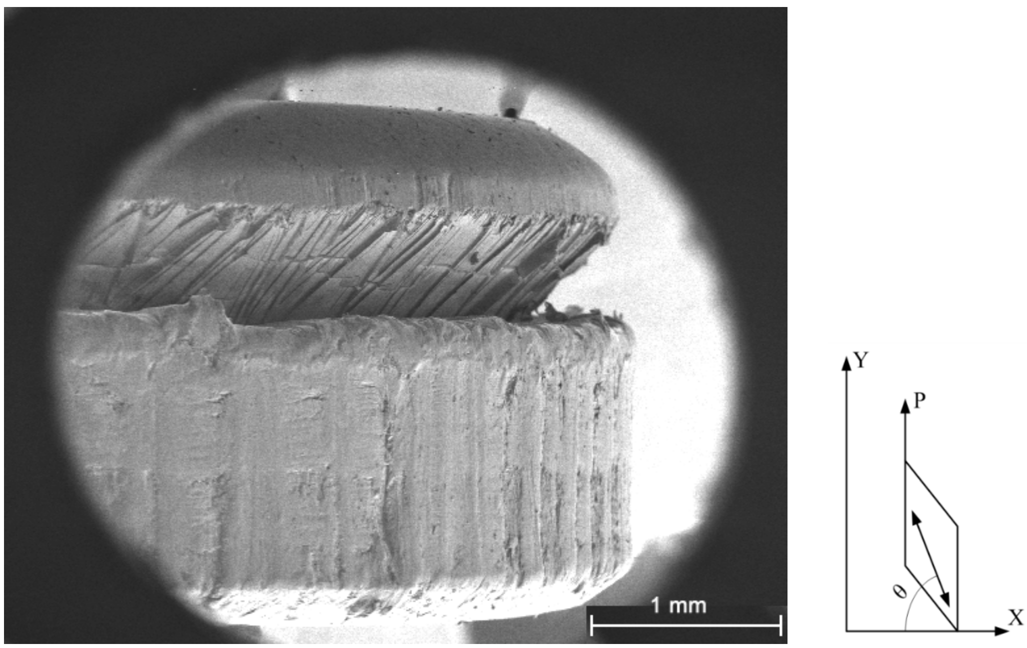

Figure 8. SEM image of a tested specimen (The global load is along Y direction).

4. FINITE ELEMENT ANALYSIS

4.1 Finite Element and Material Models

Figure 9 shows the finite element mesh used in this study employing four node axisymmetric elements. The geometry parameters are shown in the figure. Throughout this study, $r_0 = 5.5\,mm$, $R_s = 31.5\,mm$, $h = 3\,mm$ are used for the finite element analysis. In addition, to identify the influence of the punch tool clearance, three different cases are simulated with $\delta = 0.05h, 0.1h, 0.15h$. Note that for different δ, the global geometry of the specimen is unchanged by keeping $R_0 + \delta = 12.7\,mm$. It should also be noted that the outer portion of the specimen is fixed in the axial direction and the displacement load is applied to the central portion by specifying an identical displacement for both the upper and lower surfaces. As illustrated in the figure, finer mesh is employed for the shearing zone corresponding to the clearance and the final mesh density is determined by a mesh convergence study.

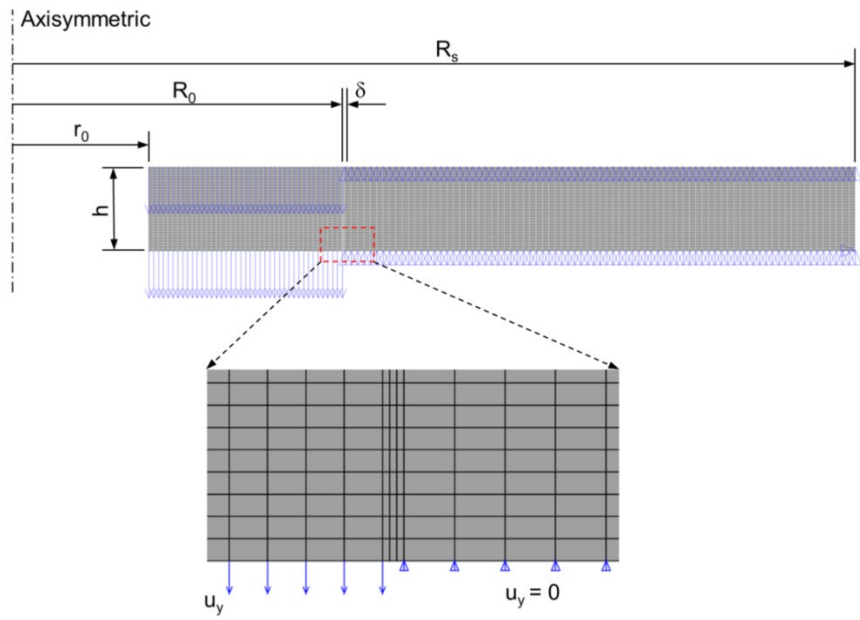

Figure 9. Axisymmetric finite element mesh and constraints.

The present study focuses on the quasi-static response in punch shear. Hence a bilinear elastic-plastic (kinematic hardening) material model is employed to simulate the nonlinear behaviour of polycarbonate. The material properties used are: elastic modulus $E = 1000$ MPa (secant modulus), Poisson's ratio $\nu = 0.37$, yield stress $\sigma_0 = 50$ MPa, and the hardening modulus $H = 60$ MPa. Figure 10 shows the material model and a comparison with the test data reported in literature [17-18].

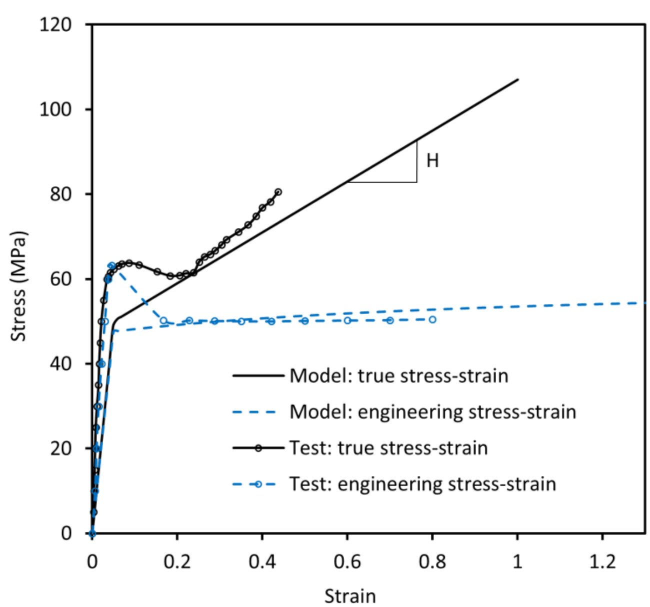

Figure 10. Bilinear elastic-plastic material model.

To verify the material model and material constants employed, a plane simple shear test reported by G'Sell and Gopez [19] was analyzed using the finite element method assuming a uniform deformation mode. Figure 11(a) shows the dimensions of the rectangular material block in shear. To reach the uniform shear deformation, the following displacement boundary conditions are imposed to the rectangular material block [19] shown in Figure 11(a).

$$\text{On plane } ABCD\text{:}\ u_x = 0, u_y = 0 \quad [12]$$

$$\text{On plane } EFGH\text{:}\ u_x = 0, u_y = 8 \quad [13]$$

$$\text{At point } A\text{:}\ u_z = 0 \quad \text{(to eliminate rigid body motion)} \quad [14]$$

The rectangular block is meshed with 10 brick elements stacking in the Y direction. Moreover, the loading displacement is specified incrementally in 300 equal steps and the average shear stress is evaluated by the load corresponding to the displacement and the area in shear by

$$\bar{\tau} = \frac{P}{3 \times 60} \quad [15]$$

Figure 11(b) displays the predicted average shear stress versus the normalized displacement curve along with the test results [19]. As shown in the figure, the predicted average shear stress curve agrees well with the test result. The local shear stress also agrees well with the average shear stress at low load levels, but drops significantly at higher loads. Therefore, at large deformation levels, the average shear stress may not represent the actual shear behaviour of the material.

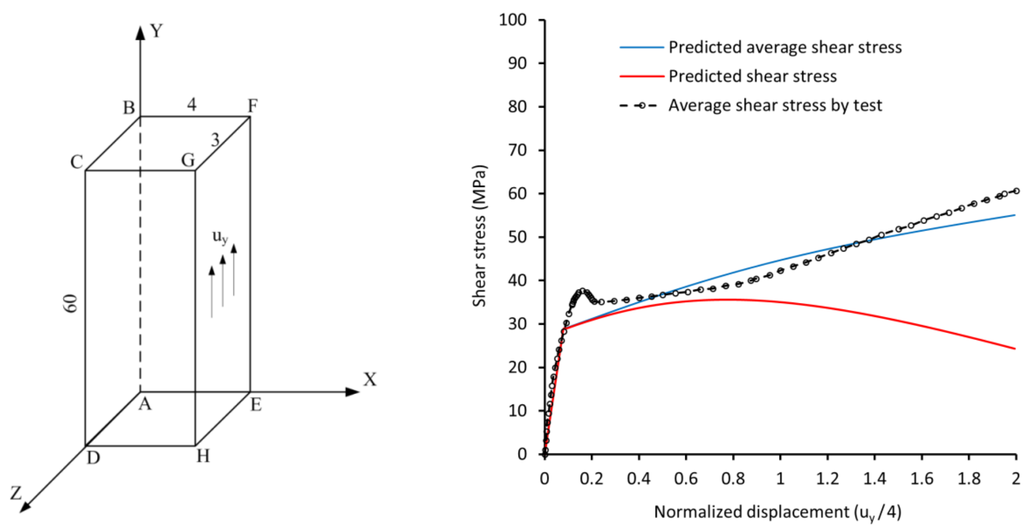

(a) (b)

Figure 11. (a) A rectangular polycarbonate block in plane simple shear (dimensions in mm); (b) Predicted response of plane simple shear and comparison with test results [19].

4.2 Results of Finite Element Analysis

Figure 12 plots the predicted average shear stress ($\bar{\tau}$) versus the normalized displacement (u_y/h) curves for the cases of $\delta = 0.05h, 0.1h, 0.15h$ along with the test results (see Figure 2). The average shear stress in the axisymmetric scenario is determined by

$$\bar{\tau} = \frac{P}{2\pi R_0 h} \quad [16]$$

where P is the resultant force on the central part of the specimen. As can be seen from the figure, the predicted average shear stress curve consists of two parts: an almost linear part up to an average shear stress of about 30 MPa and a subsequent part up to 55 to 70 MPa (for different δ) at a reduced stiffness. The calculation is terminated at $u_y/h = 0.667$, at approximately the same loading level as in the test. It is noticed that the punch tool clearance has a considerable influence on the shear response. At $u_y/h = 0.667$, the predicted average shear stresses are 71.0 MPa, 67.2 MPa, and 61.9 MPa, for $\delta = 0.05h, 0.1h,$ and $0.15h$, respectively. Finally, as shown in the figure, the predicted average shear stress curves agree well in trend with the available test results for almost the entire displacement range.

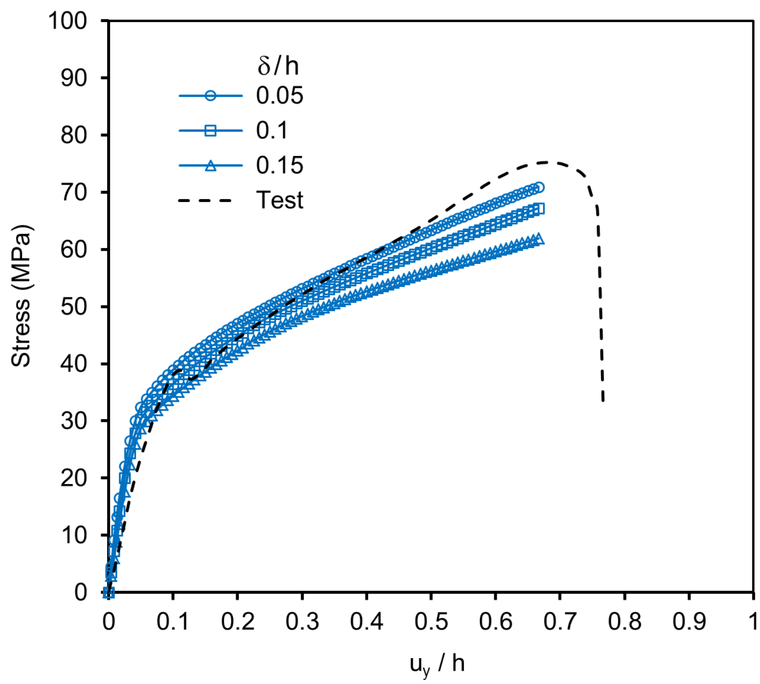

Figure 12. Predicted and test results.

Figure 13(a) displays the predicted shape of the deformed specimen at displacement of $u_y/h = 0.25$, for the case of $\delta/h = 0.1$. The contour of the first principal strain is also depicted in the figure to illustrate the deformation zone. It is noted that the first principal strain $e_1 = ln\lambda_1$, where λ_1 is the first principal stretch as defined in Equation [8]. It can be seen from Figure 13(a) that the deformation is localized in the zone around the punch tool clearance, as expected.

Figure 13(b) represents the distribution of the first principal strain at $u_y/h = 0.25$ (a magnified image of Figure 13a). The location of the maximum principal strain is indicated by the arrows in the figure. Assuming the first principal strain damage criterion, damage could occur if the principal strain exceeds the failure strain. An example of the damage produced during the punch shear test is demonstrated in Figure 8.

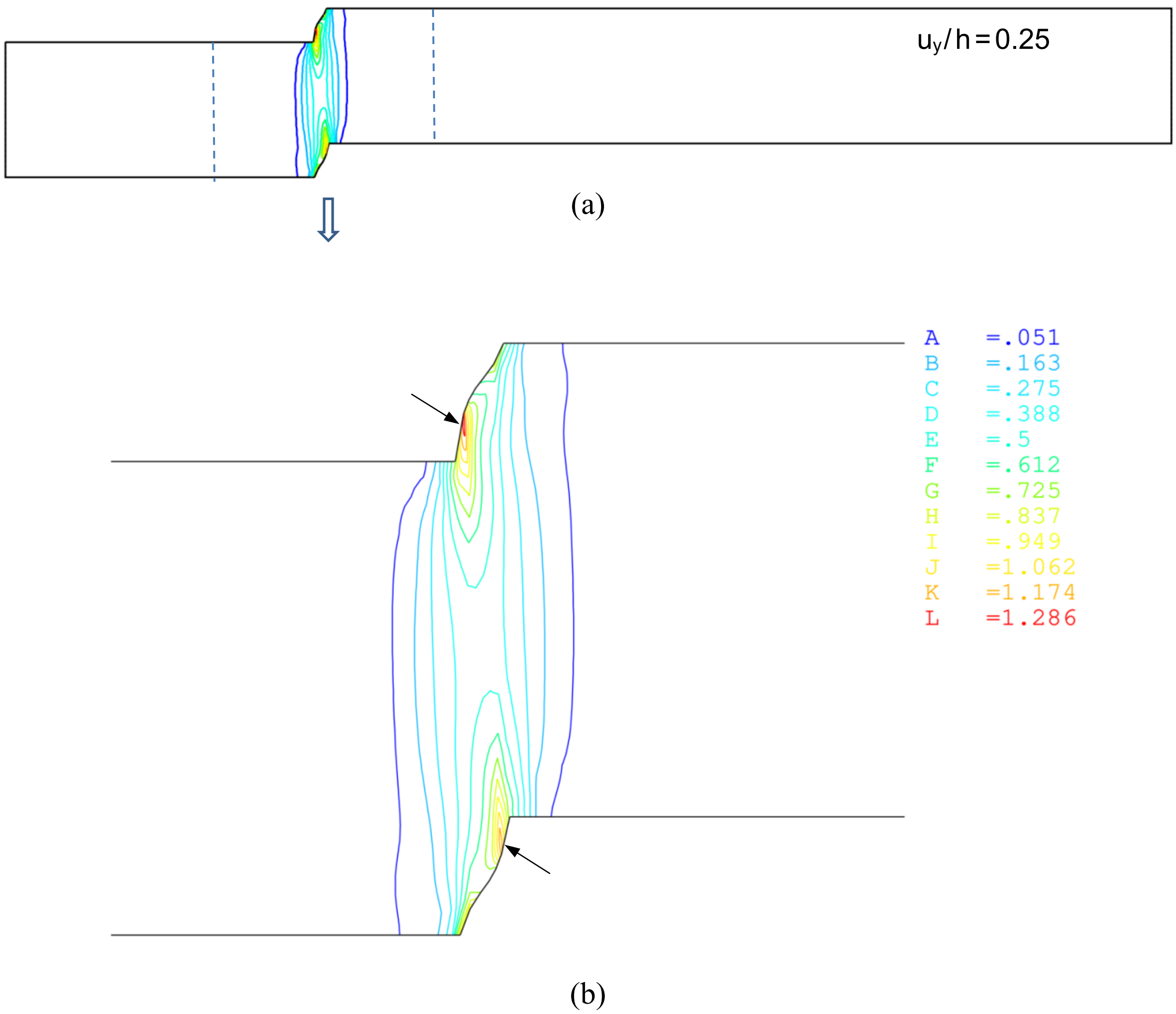

Figure 13. (a) Deformed specimen; (b) Distribution of the first principal strain.

As shown in Figure 12, there is an apparent "yield" point at approximately $u_y/h = 0.05$ in the average shear stress versus the normalized displacement curve. To illustrate the (local) plastic deformation behaviour around the yield point, Figures 14 (a), (b), (c) and (d) demonstrate the distribution of the equivalent plastic strain at $u_y/h = 0.025,\ 0.049,\ 0.05,$ and 0.1, respectively. As shown in the figure, local plastic deformation occurs at $u_y/h = 0.025$ in the predicted average shear stress versus the normalized displacement curve, well before the apparent "yield" point (Figure 14a). As the load increases to $u_y/h = 0.049$, the plastic zone expands toward the centre of the specimen (Figure 14b). And slightly further at $u_y/h = 0.05$, the plastic zone expands to the entire thickness of the specimen (Figure 14c). Further loading will expand the plastic zone primarily in the radial direction, as demonstrated in Figure 14(d).

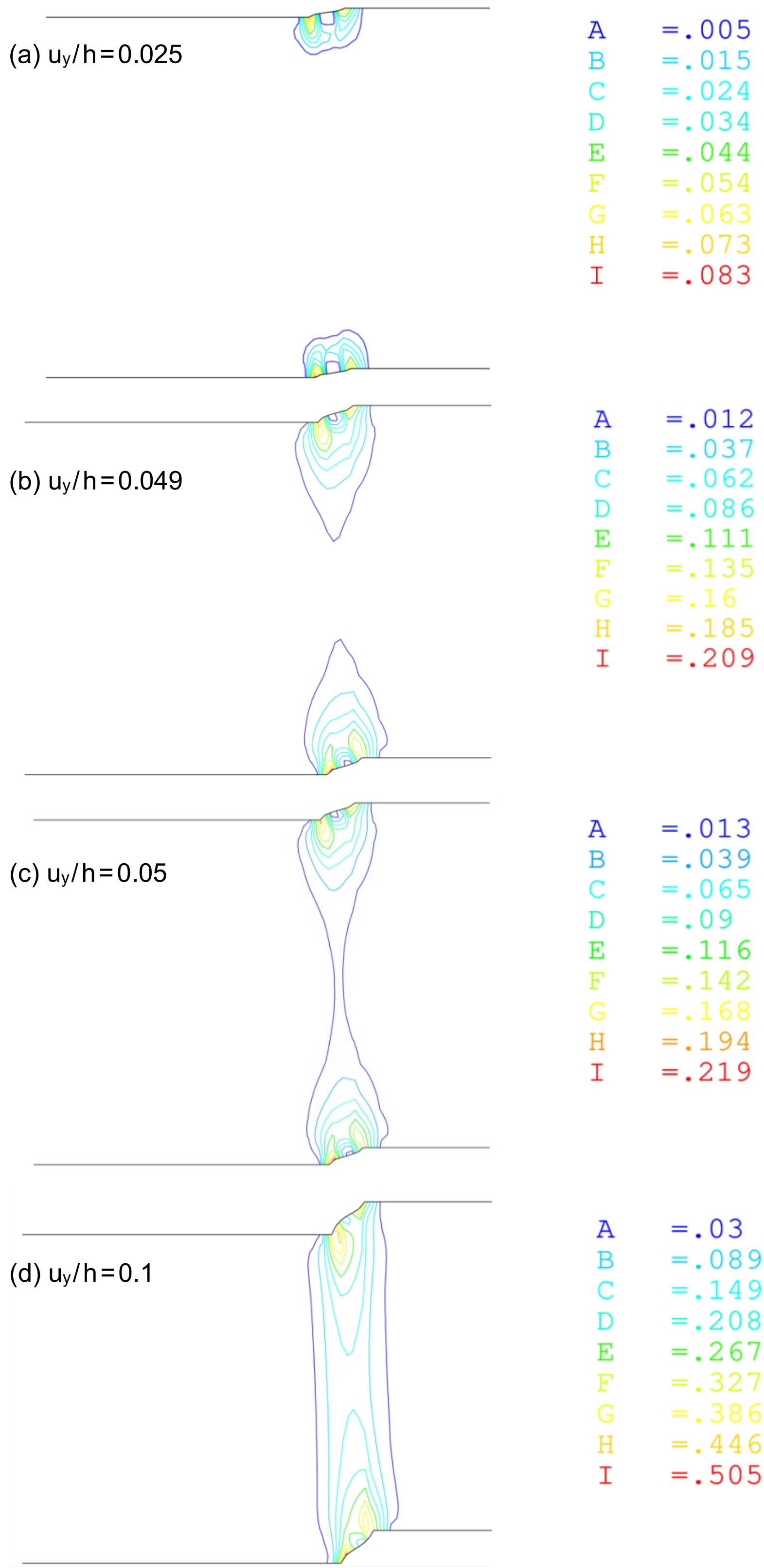

Figure 14. Evolution of the equivalent plastic strain.

5. CONCLUSIONS

The following conclusions can be drawn from the present experimental, analytical and numerical investigations:

- Ductile behaviour of polycarbonate was demonstrated and characterized by the punch shear test using disk specimens. The punch process consists of an elastic stage, a prolonged deformation stage, and an abrupt shear-out stage at large displacement.
- With the aid of scanning electron microscopy, the complex damage mode was observed. In particular, it was found that a tensile type crack existed in the punched-out specimen, indicating that tensile deformation played an important role in the punch process.
- An axisymmetric model was established assuming a uniform simple shear deformation mode. The kinematic analysis indicates that significantly large shear and normal strains exist at high load level, confirming the test observation that both tensile and shear damages can occur during punch shear.
- A nonlinear finite element analysis accounting for the large deformation effect was performed. Numerical results demonstrated that the punch tool clearance had a considerable influence on the punch shear response and the predicted results of average shear stress versus normalized displacement curves were in good agreement with the test results.
- It was demonstrated that the potential damage location can be identified using the principal strain damage criterion. Moreover, plastic deformation may occur well before the apparent yield point in the average shear stress versus displacement curve.

6. REFERENCES

1. Legrand, G.D., Bendler, J.T. *Handbook of Polycarbonate Science and Technology*. Marcel Dekker, New York, USA. 2000.
2. Driscoll, S. (editor). *The Basics of Testing Plastics: Mechanical Properties, Flame Exposure, and General Guidelines (ASTM Manual Series: MNL35)*. ASTM International, West Conshohocken, PA, USA, 1998.
3. ASTM Standard D732-17, 2017, "Standard Test Method for Shear Strength of Plastics by Punch Tool" ASTM International, West Conshohocken, PA, 2017, DOI: 10.1520/D0732-1710, www.astm.org.
4. Liu, K., Piggott, M.R. "Shear Strength of Polymers and Fiber Composites: 1. Thermoplastic and Thermoset Polymers." *Composites* 26 (1995): 829-840. https://doi.org/10.1016/0010-4361(95)90876-2
5. Liu, K., Piggott, M.R. "Fracture Failure Processes in Polymers. I: Mechanical Tests and Results." *Polymer Engineering and Science* 38 (1998): 60-68. https://doi.org/10.1002/pen.10165
6. Liu, K., Piggott, M.R. "Fracture Failure Processes in Polymers. II: Fractographic Evidence." *Polymer Engineering and Science* 38 (1998): 69-78. https://doi.org/10.1002/pen.10166
7. Mitsomwang, P., Nagasawa, S. "Effects of Shearing Parameters on Cutting Characteristics of Polycarbonate Sheet Subjected to Straight Punch/die Shearing." *Journal of Materials Processing Technology* 220 (2015): 46-57. https://doi.org/10.1016/j.jmatprotec.2015.01.007

8. Husain, A., Ansari, R., Khan, A.H. “Experimental and Numerical Investigation of Perforation of Thin Polycarbonate Plate by Projectiles of Different Nose Shape.” *Latin American Journal of Solids and Structures* 14(2017): 357-372. http://dx.doi.org/10.1590/1679-78253252
9. Bilyk, S.R. “A Computational Analysis of a Shear Punch Test.” *Proceedings of the JANNAF Conference*. Colorado Springs, CO, 1-5 December 2003.
10. Lee, S-W. R., Sun, C.T. “A Quasi-Static Penetration Model for Composite Laminates.” *Journal of Composite Materials* 27(1993): 251-271. https://doi.org/10.1177/002199839302700302
11. Nemes, J.A., Eskandari, H., Rakitch, L. “Effect of Laminate Parameters on Penetration of Graphite/Epoxy Composites.” *International Journal of Impact Engineering* 97 (1998): 97-112. https://doi.org/10.1016/S0734-743X(97)00026-2
12. Gama, B.A., Gillespie, J.W. “Punch Shear Based Penetration Model of Ballistic Impact of Thick-section Composites.” *Composite Structures* 86(2008): 356-369. https://doi.org/ 10.1016/j.compstruct.2007.11.001
13. Boyce, M.C., Arruda, E.M., Jayachandran, R. “The Large Strain Compression, Tension, and Simple Shear of Polycarbonate.” *Polymer Engineering and Science* 34 (1994): 716-725. https://doi.org/10.1002/pen.760340904
14. Varghese, A.G., Batra, R.C. “Constitutive Equations for Thermomechanical Deformations of Glassy Polymers.” *International Journal of Solids and Structures* 46 (2009): 4079-4094. https://doi.org/10.1016/j.ijsolstr.2009.08.006
15. Chadwick, P., *Continuum Mechanics, Concise Theory and Problems*, Dover, Mineola, New York, 1999.
16. Kurtz, S.M., Jewett, C.W., Bergström, J.S., Foulds, J.R., Edidin, A.A. “Miniature Specimen Shear Punch Test for UHMWPE Used in Total Joint Replacements.” *Biomaterials* 23 (2002): 1907-1919. https://doi.org/10.1016/S0142-9612(01)00316-7
17. Cao, K., Wang, Y., Wang, Y. “Experimental Investigation and Modeling of the Tension Behavior of Polycarbonate with Temperature Effects from Low to High Strain Rates.” *International Journal of Solids and Structures* 51 (2014): 2539-2548. https://doi.org/ 10.1016/j.ijsolstr.2014.03.026
18. Knapp II, K.N., Gabriele, G.A, Lee, D. “Stress-strain Response of Polymers for Predicting the Behavior of Integral Fasteners”. *ANTEC '97 Conference Proceedings*, Society of Plastic Engineers Annual Technical Conference and Exhibit. Toronto, Canada, April 27-May 2, 1997. pp. 1198-1202.
19. G'Sell, G, Gopez, A.J. “Plastic Banding in Glassy Polycarbonate under Plane Simple Shear.” *Journal of Materials Science* 20(1985): 3462-3478. https://doi.org/10.1007/BF01113753